Guilhabert, B., Bommer, S. P., Wessling, N. K., Jevtics, D., Smith, J. A., Xia, Z., Ghosh, S., Kappers, M., Watson, I. M., Oliver, R. A., Dawson, M. D., & Strain, M. J. (2023).
Advanced transfer printing with in-situ optical monitoring for the integration of micron-scale devices.
IEEE Journal of Selected Topics in Quantum Electronics, 29(3), 1-11. [7900111].
https://doi.org/10.1109/jstqe.2022.3227340

Advanced transfer printing with in-situ optical monitoring for the integration of micron-scale devices

Benoit Guilhabert, Sean P. Bommer, Nils K. Wessling, Dimitars Jevtics, Jack A. Smith, Zhongyi Xia, Saptarsi Ghosh, *Member IEEE,* Menno Kappers, Ian M. Watson, Rachel A. Oliver, Martin D. Dawson, *Fellow IEEE,* Michael J. Strain, *Senior Member IEEE*

***Abstract*—Transfer printing integration of planar membrane devices on photonic and electronic circuits is becoming a well established technology. Typical systems incorporate a single planar layer printed into full contact with the host substrate. In this work we present an advanced transfer print system that enables printing of optical devices in non-planar geometries and allows in-situ optical monitoring of devices. We show micro-resonators with air-clad whispering gallery modes coupled to on-chip waveguides, inverted device printing and three dimensionally assembled micro-cavities incorporating semiconductor micro-lenses and nanowire lasers. We demonstrate printing onto non-standard substrates including optical chip facets and single-mode fibre ends. The optical fibre printing was carried out with alignment assistance from in-situ optical coupling through the transfer printing system in real-time allowing active alignment of the system.**

***Index Terms*—Integrated optics, Optical waveguide components, Hybrid integrated circuits, Semiconductor device fabrication, transfer printing, photonic integration.**

I. Introduction

TRANSFER printing is rapidly maturing as a back-end integration technology for applications including telecommunications [1]–[3], quantum technologies [4]–[6], and flexible displays and electronics [7], [8]. Fully fabricated membrane devices from a donor substrate are released using selective under-etching of the membrane in a MEMs-like process [9], and subsequently transferred to a host substrate, Photonic Integrated Circuit (PIC) or electronic back-plane using an accurate pick-and-place tool [10], [11]. Usually the transfer printing integration stage includes the transfer of a planar membrane device onto a planar receiver, effectively creating one additional vertical device layer on the chip [3], [12]–[15]. Multi-material integration has been achieved in laterally distributed arrangements [16], [17] and initial mechanical proof-of-concept demonstrations of multi-layer printing have been made [18]–[20]. To fully exploit the potential of the transfer printing method, the third dimension can be better employed and this requires advances in the toolset and process methodology to allow micro-assembly of vertically structured devices on-chip.

In this paper we present the design of a custom-built transfer printing instrument and examples of a range of advanced device geometries that are enabled using this tool. In Section II we present an overview of the system design, incorporating a 6-degree of freedom motion stage, optical injection module for in-situ process monitoring, and the capability for mounting non-planar device geometries. Section III presents challenging printing demonstrations making use of competitive adhesion effects and high accuracy alignment, including micro-disk resonators printed onto micro-pillars and evanescently coupled to planar, on-chip waveguides, NW devices printed within micron-scale footprints, and a multi-stage process for inverted device printing of membrane devices. A demonstration of multi-layer printed devices and air-cavity assembly is demonstrated in Section IV where nanowire lasers are integrated with semiconductor membrane micro-lenses. Section V presents demonstration of printing onto non-standard receiver geometries including the facets of optical fibre and waveguide chips. In-situ process monitoring of device printing of micro-lenses onto optical fibre facets using optical injection both through the fibre itself and from the print tool microscope column is also presented. Finally, we summarise the potential of this process and toolset for future applications.

II. Transfer Printing Instrument

The basic methodology for transfer printing integration has been well documented [10], [19], [21] and relies on the pick-and-place manipulation of thin membrane devices using a soft polymer stamp, typically in Polydimethylsiloxane (PDMS), to detach them from their native substrate and deposit them onto a host substrate or circuit. The surface adhesion of the PDMS stamp can be coarsely tuned during the mixing stage by varying the ratio of the oligomer base formulation to curing agent in the mixture. Higher ratios of oligomer base formulation to curing agent result in more flexible and adhesive surfaces [17] and a ratio of 10:1 (Sylgard 184 [22]) is a common mixture for working with micron scale, flat membrane devices. The transfer printing tool generally consists of a high resolution translation stage on which the samples are mounted, a rigidly mounted stamp holder and an optical microscope rigidly connected to the supporting base

B. Guilhabert, S. Bommer, N.K. Wessling, D. Jevtics, J.A. Smith, Z. Xia, I.M. Watson, M.D. Dawson and M.J. Strain are with the Institute of Photonics, University of Strathclyde, 99 George street, Glasgow G1 1RD, UK. *B. Guilhabert, S. Bommer, N. Wessling and D. Jevtics contributed equally to this work.*

S. Ghosh, M. Kappers, R.A. Oliver are with the Cambridge Center for Gallium Nitride, University of Cambridge, Cambridge CB3 0FS, UK

Manuscript received August 1, 2022; revised August xx, 2022.

table, allowing imaging through the transparent stamp to the donor and receiver substrates on the translation stage. In this way the donor and receiver samples are translated in x,y,z and θ_z directions under the stamp head and printing is achieved by bringing the substrates into contact with the stationary stamp head. In our system we follow this arrangement with a few additions. Fig. 1(a) and (b) show schematic views of our transfer printing instrument. The translation stage used to control the substrate motion relative to the stamp head is a 6-axis parallel kinematic stage arrangement with nanometric relative positional accuracy and improved stiffness and rigidity over a serially combined multi-stage approach. The Minimal Incremental Motion (MIM) of the stage system is 5 nm in x, y and z directions and less than 1 μrad in rotation in θ_x, θ_y and θ_z. The full travel range of the stage system is 200 mm in the x and y directions, 10 mm in the z-direction, with a θ_x and θ_x range of 6^o and a θ_z range of 20^o. The parallel kinematics makes it possible to select 6-axis stage positions - commonly referred to as stage poses - and motion paths compatible with printing onto non-planar receivers and to correct for planar alignment variations between substrates after mounting onto the stage, a particular concern when printing over large spatial areas. The stamp holder and the microscope system are mounted in a rigid connection with the base table. Furthermore, the microscope head used to image through the stamp is mounted on a movable rail that can be locked into position for a consistent field-of-view (FOV) position during printing. Automated control of the alignment process for donor and receiver chips and development of a fully integrated software control system for device alignment and printing stages has improved full process times from ≈ 30 mins in earlier systems [23]to only a few minutes for the full setup, alignment and print process.

A further addition to the microscope head is the integration of an optical injection line that allows for the coupling of light sources onto the print surfaces. The column comprises a fibre coupling port, parabolic mirror collimator, galvanometer beam steering element, a scan and tube lens configuration and beam-splitter, as shown in Fig. 1(b). In this way, a fibre-coupled optical source can be imaged onto the focal plane of the microscope imaging objective, with the spot position being controllable to sub-micron accuracy using the galvo-scanner and real-time monitoring of the microscope camera. A variety of wavelengths can be employed in this system for applications from in-situ photocuring, or optical coupling to on-chip devices during the print cycle. Details of the in-situ monitoring operation are presented in Section V.

As noted above, the microscope is movable to allow monitoring of larger sample areas outwith the field-of-view in the central print area, and to aid tilt compensation and wider area monitoring for large scale printing. The tilt correction can be actively controlled using optical microscopy feedback employing polymer stamp heads with large arrays of surface points that can be brought into contact with a substrate, as shown in Fig. 2. The substrate is mounted onto the stage and raised towards the stamp head in small steps. When one of the pyramidal PDMS projections makes contact with the substrate its surface deforms creating a planar contact between

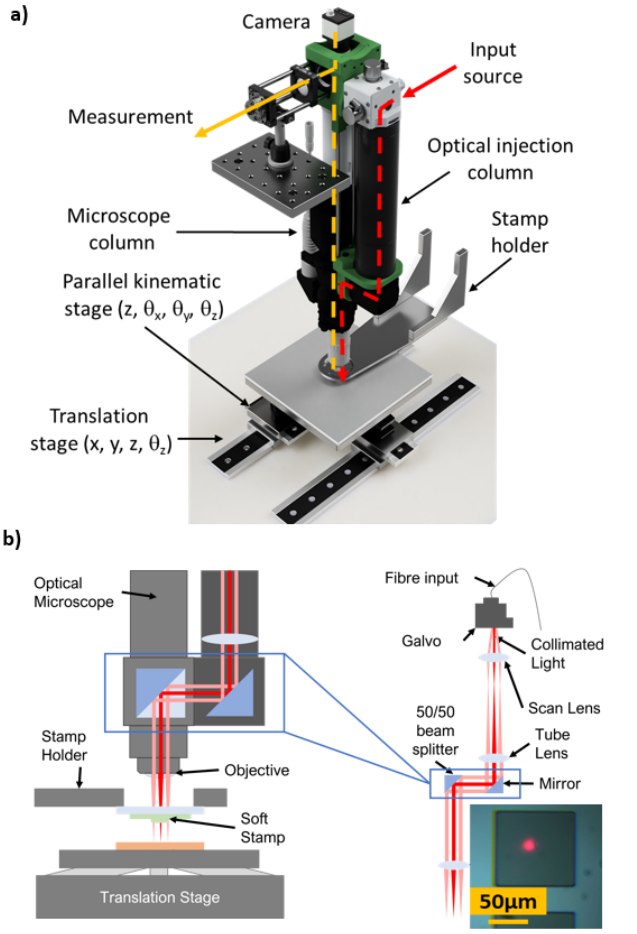

Fig. 1. (a) Schematic of the custom transfer printing instrument and (b) optical injection column. Inset shows laser spot imaged onto a sample surface in-situ.

the polymer and substrate, increasing light reflected into the microscope. In Fig. 2(a) most of the polymer protrusions are not in contact with the substrate, and as shown in the magnified image, the protrusion area appears dark. The associated histogram shows a measurement of the number of points of contact within the field of view. The protrusions are numbered from the top left of the microscope images in a raster fashion, column-wise, for the histogram results presented in Fig. 2. As the substrate deforms the protrusions, an automated image processing tool allows for calculation of the contact area based on the appearance of a central bright area in the dark square of the pyramidal head. The area of this bright spot is directly related to the contact force between the stamp and substrate and so can be used as a rough measure of the local substrate vertical displacement. The vision system maps the relative displacement of the contact point array as a function of position and calculates the plane rotation required to compensate for relative rotations between the stamp and substrate. Finally, this relative rotation in 2-axes can be compensated for by modifying the stage pose. This compensation is carried out for all substrates being used in the printing process. Contact between the compensated substrates and stamp then shows uniform distribution of contact across the protrusion array above a threshold value of contact area, denoting full contact

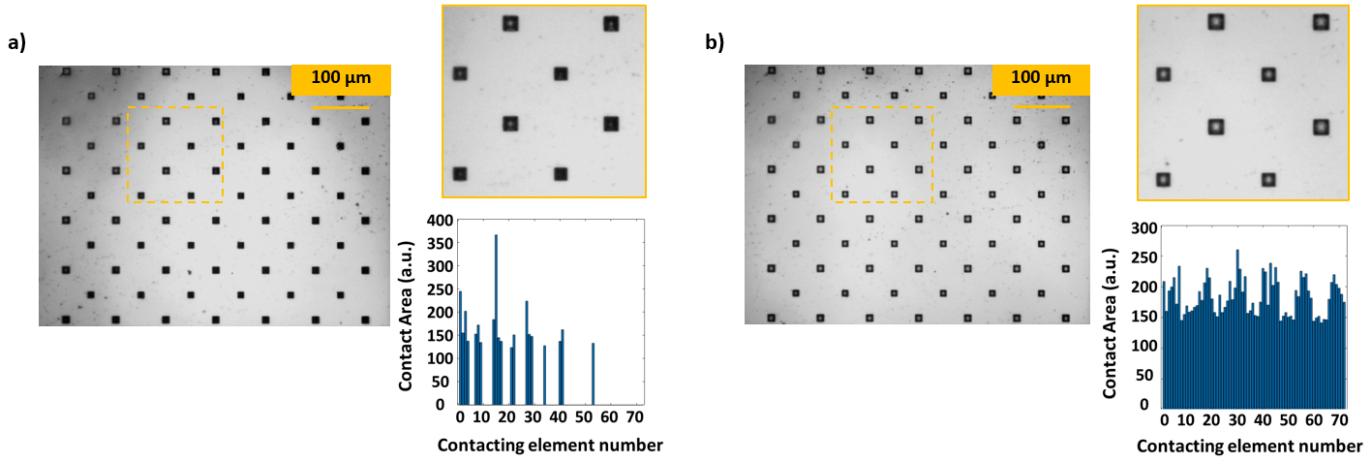

Fig. 2. (a) Microscope image of an array of pyramidal contact features on a PDMS stamp contacting a test substrate and histogram of the number of points in contact in the microscope field of view in that case. (b) Microscope image of the contact point array after 2-axis compensation showing improved uniformity of contact and associated histogram of extracted contact points. (Insets show magnified images of the contact points with bright areas within dark squares indicating deformation of the pyramidal features in contact with the substrate.)

of individual points, as shown in Fig. 2(b). For stamp heads to be used for device-specific printing, either the pickup points themselves can be used for this compensation process, offset from the pickup locations, or ancillary contact points can be distributed across the pickup head area to perform this function.

The following sections detail transfer printing processes and device geometries enabled by the development of this toolset.

III. Competitive Adhesion Effects for Challenging Printing Applications

Transfer of membrane devices from a donor to receiver substrate using a polymer stamp typically makes use of competitive adhesion effects between the various surfaces and micro-fabricated stamps. For planar-to-planar device contact, and where adhesion-promoting layers on the receiver are used, this is a relatively simple process relying on velocity control of the stamp relative to the donor or receiver [19]. In general, a fast stamp retraction from the donor leaves the membrane attached to the stamp and a slow retraction from the receiver leaves the membrane on the receiver. The particular formulation of PDMS required for reversible adhesion, stamp head profile and motion control settings for pickup and release, are all optimised for each particular device material and geometry based on an iterative trial process. There are however application cases where serial printing of multiple devices into dense arrangements is required, where multi-stage printing is necessary, or where devices are required to be printed onto suspended geometries with contact regions down to μm^2 areas. This presents a challenge to the process that can be addressed by appropriate stamp design, material composition or process flow. Examples of suspended devices, dense device integration and flipped membrane printing are presented here.

A. Reduced contact area printing for suspended devices

As noted in the introduction, transfer printed membrane devices are typically planar devices with a full contact surface area between the printed device and substrate. In some applications it is desirable to have waveguide regions suspended in air, either to enable modal overlap with a sensing region, or to avoid substrate losses in ultra-high Q-factor resonators [24] or mid-IR transmission waveguides [25]. Suspended resonator or cantilever devices are typically fabricated on their native substrate using a selective underetch and then optically coupled using tapered fibre [26] or with free-space optics [27]. Here in a relevant example, we present printing of micro-disk resonators onto micro-pillars, so that the area of contact is less than the total disk area, see Fig. 3(a). The micro-resonators can then be printed with their waveguiding region suspended in air, but with a spatial overlap to an on-chip waveguide to allow optical coupling to the resonator. Our previous demonstrations of printed full-contact micro-disk resonators have shown that the spatial accuracy in the 100 nm range required for waveguide-to-waveguide coupling is possible and that the extra degree of freedom enabled by the vertical separation and lateral spacing of the optical structures allows for selective mode coupling [28], [29].

Fig. 3(a) shows a schematic of the integration of aluminium gallium arsenide (AlGaAs) micro-disks onto micro-pillars. The proximity of the suspended microdisk edge and polymer on-chip waveguide enables evanescent field coupling between the two. The micro-disk resonators are 20 μm in diameter and the polymeric waveguides are 3 μm in width and have a height of 2.5 μm. In order to create a well defined vertical air gap between the bottom surface of the micro-disk and the top surface of the polymer waveguide, the micro-pillars can be fabricated on a shallow pedestal etched into the substrate, creating a positive step relative to the area the waveguides are defined on. The SU8 polymer for the waveguides and micro-pillars can be fabricated in a single lithography stage by spin coating and exposure using direct write laser lithography. The micro-pillars are 10 μm in diameter presenting a print contact area that is a quarter of the surface area of the micro-disks, thus providing a dramatically reduced surface for the device to

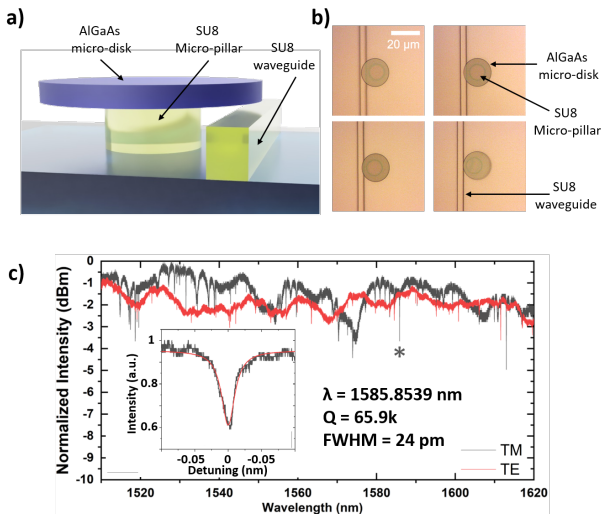

Fig. 3. (a) Schematic of an AlGaAs micro-disk resonator printed onto a micro-pillar and in proximity to a polymer waveguide. (b) Optical microscope images of printed micro-disks where the lateral separation between the resonator edge and the edge of the on-chip waveguide as a parameter. (c) Measured transmission spectra of a waveguide coupled micro-disk resonator for TE and TM polarisations. The inset shows detail of a single resonant peak (marked by an asterisk) and extracted device parameters.

adhere, impacting on the TP competitive adhesion behaviour between receiver surface and stamp. A combination of low-adhesion stamp material and control of the stamp release velocity allows for the successful deterministic placement of the resonators onto the micro-pillars [17]. Several micro-disk resonators were printed where the lateral separation between the edge of the micro-disks and the polymer waveguide edge was used as a parameter to demonstrate varying optical mode coupling, as shown in the micrographs in Fig. 3(b). Four variations are shown, reducing in optical mode overlap, including alignment of the micro-disk edge point to (1) the lefthand side waveguide edge (top left, Fig.3(b)), (2) the centre of the waveguide (top right, Fig.3(b)), (3) 0.75 μm from the righthand waveguide edge (bottom left, Fig.3(b)) and (4) the righthand waveguide edge (bottom right, Fig.3(b)).

Transmission measurements of the micro-disks were taken using a swept wavelength laser source as detailed in [29]. Sample transmission measurements for both TE and TM injection polarisation are shown in Fig. 3(c) for the highest extinction resonance device, corresponding to the device shown in the bottom left image of Fig.3(b). Curve fitting of the selected resonances [30] demonstrates loaded Q-factors of up to 65k for fundamental TM modes and an example fitted resonance is shown in the inset to Fig. 3(c).

B. Serial printing of nanowire devices

As detailed in [17] there are two main challenges associated with transfer printing of nanowire (NW) devices. The first is the small contact area between the nanowire surface and the receiver substrate, which makes the competitive adhesion between the transfer stamp and receiver surface challenging to engineer in favour of the receiver. The second challenge for serial printing of ultra-compact devices within micrometre

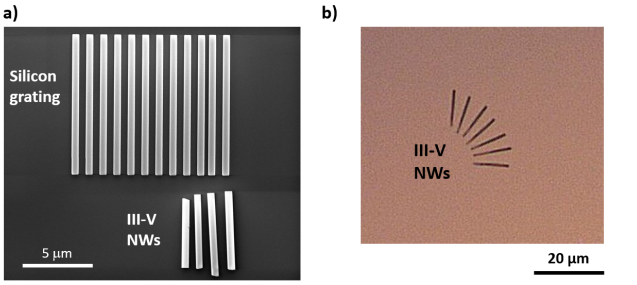

Fig. 4. (a) SEM image of NW devices printed with their major axes aligned with a lithographically defined silicon grating with 500 nm linewidth. (b) Optical microscope image of serially printed nanowire devices in a densely arrayed format.

scale footprints is that the transfer stamp will come into contact with previously printed devices in subsequent transfer runs. The deterministic transfer of NW devices has been addressed by us in a recent review, where a number of complementary techniques are discussed [31]. Deterministic transfer printing of single NW devices has been demonstrated with absolute accuracy in the few hundred nanometres range [23], [31]. In the case of serial transfer printing of multiple NWs in close proximity, a two-stage printing process can be employed to address the repeatable release of devices onto the receiver and the challenge of avoiding re-pick up of pre-printed devices. Inter-device spacing can be accurate to within a few hundred nanometres with minimum separation distances around 1 μm [17].

First, the NW devices are transferred from their growth substrate to an intermediate substrate with low surface adhesion and where the NWs are randomly distributed. The PDMS stamp is then fabricated using a base to curing agent ratio of 8:1 to produce a reduced surface adhesion as compared with typical stamp designs using a 10:1 ratio. The selected NWs are then transferred to a receiver substrate with sub-nanometre surface roughness using the 8:1 PDMS stamp. The adhesion competition between the 8:1 stamp and the low roughness receiver favours the receiver in a slow stamp release process, allowing transfer of the NWs with high spatial accuracy. By using automated image processing tools to locate the position and orientation of the NW within the microscope field of view, and relative to the transfer stage position, these devices can be printed with absolute positional accuracy in the few hundred nanometres range [23], [31]. Fig. 4(a) shows an SEM image of four NWs transferred onto a silicon substrate in this way, where the silicon lines are 500 nm wide and the NWs were printed in a serial process. In the serial process the stamp head comes into contact at each printing stage with devices already deposited on the receiver, but by using the slow release and reduced adhesion stamp formulation, existing devices are not removed or shifted during each print cycle. Fig. 4(b) shows an array of NWs printed into a compact arrangement with their axes forming radial lines over a relative rotation angle of 90^o. This process showed robustness to 6 additional print cycles after transfer of the first NW.

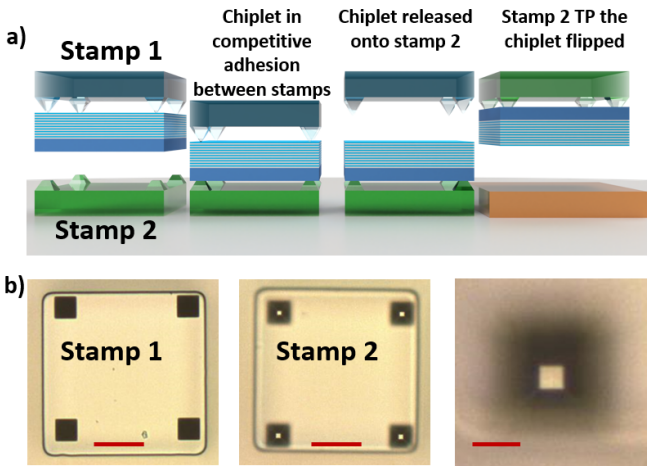

Fig. 5. (a) Schematic of the flipped transfer print process. (b) Optical microscope images of the two stamps employed in the flipped printing process, showing the full pyramidal tips of stamp 1 (left) and the flat apex pyramid in stamp 2 (middle, scale bars 20 μm). A close-up micrograph of one apex of stamp 2 is shown in the right hand image (scale bar 5 μm).

C. Inverted membrane transfer printing

Since the transfer printing process is a form of pick-and-place integration, the membrane devices retain their top surface orientation from the donor to receiver substrates, i.e. the top surface during fabrication of the donor membrane remains the top surface after printing. It can be advantageous to decouple the growth and fabrication membrane orientation from the final device placement, for example to allow direct electrical connection of metal contacts deposited on membrane devices with contact tracks on the receiver substrate. To allow this inverted or 'flipped' device printing, an intermediate stage can be added to the process as detailed in Fig. 5(a). This process uses two stamp head chips and in the initial configuration stamp head 1 is mounted into the transfer print tool in the usual position, while stamp 2 is placed on the translation stage as an intermediate receiver substrate. The device to be transferred is picked up from its native substrate by stamp 1 as in the standard process. Stamp 1 is then aligned over the temporary receiver (stamp 2), and the device is released onto stamp 2 using competitive adhesion. There are two major advantages gained by using stamp 2 as an intermediate receiver. Firstly, the spatial arrangement of transfer devices can be varied between the donor and final receiver substrates. i.e. the device picked up from the donor can be placed in an arbitrary location on stamp 2 before the final transfer process, providing significant flexibility in the process. Secondly, multiple donors can be used to populate stamp 2, allowing for a single shot, parallel printing of arbitrarily arranged, multiple material devices onto the final receiver with just a single print process from stamp 2.

A critical element in this methodology is that the secondary stamp should have a higher adhesion to the membrane devices than the primary stamp. To achieve this differential adhesion there are two methods available: tuning the material properties of the stamp, for example as has been shown in the case of nanowire lasers, as described in Section III above, or by varying the topology of the stamp itself. For the results presented here a topology approach is employed. Two sets of stamp heads were fabricated using a micro-fabricated PDMS mould process as detailed in [18]. Two separate stamp moulds were designed based on a pillar with pyramidal protrusions commonly used to facilitate reversible adhesion during the pick-up and release processes. The first stamp features 4 full pyramidal structures at the corners. The second, which acts as the secondary stamp in the inverting process, follows the same design but the pyramidal features are truncated so that the apex of the structures are a square area, approximately 2.5 $\times$2.5 μm^2, and importantly, larger than the contact area of the first, as shown in Fig. 5(b). To release the membrane device onto the second stamp, a similar technique to the usual transfer printing release is employed, i.e. a low velocity separation motion in the vertical direction. The adhesion between each stamp and the membrane device is directly proportional to the surface contact area and therefore will leave the device attached to the secondary stamp.

Fig. 6 presents the flipped printing process as applied to a single gallium nitride-based light-emitting diode (LED). The membrane LEDs were pre-fabricated from GaN-on-Si in a suspended fashion, as described previously in [32], with lateral dimensions of 100x100μm^2. They comprise a recessed contact to access the n-doped GaN, and a 100 nm-thick palladium (Pd) spreading layer over the p-doped GaN mesa region of the membrane. The overall membrane thickness is 3.5 μm. As shown in Fig. 6(a), the membrane is first picked up from the donor substrate and imaged through the polymeric stamp. The stamp loaded with the membrane is shown in Fig. 6(a) after the polymer has been allowed to relax and the membrane is suspended from the points of the stamp protrusions. Fig. 6(b) shows a top side image of the LED after transfer to stamp 2, i.e. the stamp is being imaged through the LED membrane. The inset of Fig. 6(b) shows the truncated pyramidal stamp feature imaged through the LED material. Fig. 6(c) and (d) show microscope images of the membrane LED prior to, and after the inverted printing process respectively. In Fig. 6(d) the top metal contact layers are visible through the transparent GaN material. The two diagonal lines are residual wet etch features on the membrane 'back-side' that are not visible through the top metal contact when the device is in its as-fabricated orientation.

IV. Vertical assembly of multiple devices: micro-lens coupled nanowire lasers

As previously noted, mechanical assembly of silicon multi-layers has been achieved by transfer printing [19], and some work has been done to show transfer printing of functional optical devices by serial stacking of structured layers using nanoprobes and in-situ electron microscopy monitoring [20], [33]. Printing of devices in suspended geometries has also been shown using micro-disks as detailed above and in [27], as well as in cases where the membrane bridges two support structures [19], [34]. The ability to suspend a membrane device above a substrate enables the formation of an air void between the two surfaces that can act as an optical cavity or provide

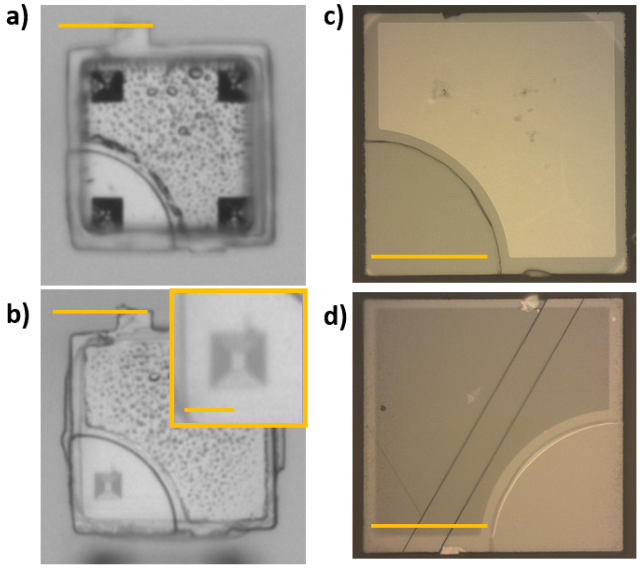

Fig. 6. Flipped transfer printing demonstration in the case of a membrane GaN LED. (a) LED membrane imaged through stamp 1 in a relaxed state. Scale bar is 50 μm. (b) Flipped LED membrane imaged through stamp 2 with truncated pyramidal features (Scale bars are 50 μm). Inset shows a magnified view of the pyramidal feature of stamp 2 (Scale bar 10 μm) imaged through the device. Final printed LED membranes on the receiver substrate using (c) the traditional single print method and (d) the inverted printing method. Scale bars are 50 μm.

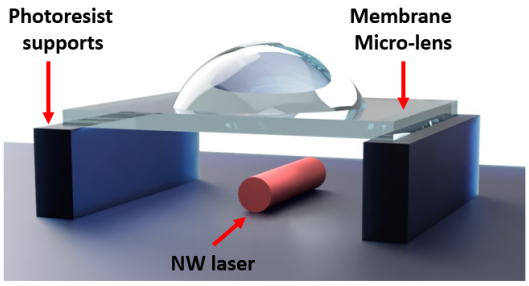

Fig. 7. Schematic view of the vertically assembled micro-lens on nanowire laser devices.

the potential for vertical integration of multiple micron scale devices, from different material platforms, without requiring planar contact between each layer. Here we present such a 3D arrangement of micron-scale optical devices that can only be achieved using spatially accurate, multi-layer transfer printing assembly. Fig. 7 shows a schematic of such a vertically assembled system comprising NW lasers with a hexagonal cross-section made of bulk InP material with a long axis length of 10 μm and a diameter of approximately 260 nm [17]. The nanowire (NW) laser is transfer printed onto a substrate within the bounds of support structures. A micro-lens device is then printed onto the supports, vertically separated but laterally aligned with the nanowire laser. In this arrangement the vertically coupled output scattered light from one of the nanowire laser facets can be efficiently coupled through the micro-lens device. For this application we use GaN based semiconductor micro-lens devices with micron scale radius of curvature and focal length, and large numerical aperture.

The manipulation and deterministic printing of the NWs relies on a multi-stage process [17] where the as-grown NWs are first sheared from their growth substrate with a low-adhesion PDMS stamp to form a randomly distributed population on an intermediate substrate. Individual NWs are then picked up sequentially and transferred onto a silica receiver substrate to form a selected pool of devices with registered position with respect to an alignment marker on chip. The selected population of devices is optically characterised to confirm lasing behaviour [35]. The optical characterisation was carried out using a micro-photoluminescence setup under pulsed optical injection at a wavelength of 532 nm with pulses of 0.5 ns and repetition rate of 7 kHz which can be attenuated to control the fluence applied at the pump beam focus. Since the pump laser focus spot has a FWHM diameter of $\approx$10 μm, the pump can be selectively applied to a local region of the NWs, which in this case allows for NW pumping off-axis from the micro-lens, through the membrane mesa. The vertically scattered lasing emission from the NW facet is coupled through the microscope injection system to a spectrometer (Avantes, 0.14 nm spectral resolution). Once target devices are identified the NWs are then re-printed onto a dedicated receiver chip where sets of polymer support frames in photo-resist (Shipley s1818) were fabricated with UV photolithography with fixed height of 1.6 μm. The NWs were positioned within the frame area to ensure no physical contact between the structures. The frames are then used to act as supports for the subsequent printing of the individual GaN micro-lens over selected NW facets.

The GaN micro-lenses are fabricated using a GaN/AlGaN/AlN layer stack grown on 6" Si wafers [36]. Membranes with the micro-lens are processed using a combination of laser lithography, high temperature reflow and inductively coupled plasma dry etching. Full details on the micro-lens design and fabrication can be found in [37]. The resulting micro-lens devices are then released from the growth substrate using a chemical wet etching in potassium hydroxide. The dimensions of the membranes selected for this work were squares of 17x17 μm^2 with spherical micro-lenses of 12 μm in diameter with a lens height of 3 μm. The micro-lenses were then printed in a suspended geometry onto the NW-containing frames. The individual micro-lenses are printed aligned with one facet of the NWs.

Figure 8(a) shows fabricated devices where the printed NWs can be seen located between the polymer frame supports, a magnified image is shown in Fig. 8(c). Fig. 8(b),(d) and (e) show the substrate after printing of the micro-lenses over one facet of each of the NWs. In Fig. 8(d) the microscope is set to image the substrate plane, while in Fig. 8(e) it is focused on the top surface of the micro-lens. The black line on the lens in Fig. 8(e) is a visual guide to the NW location, obtained using image overlay, showing alignment of the NW facet with the centre of the lens.

Optical characterisation of the NWs after printing into the frame structures was carried out prior to lens integration. The transferred NWs were measured with lasing wavelengths ranging from 860 to 880 nm and thresholds on the order of 10's of $\mu J/cm^2$. Fig. 9 and its inset show a representative NW lasing threshold curve and spectrum respectively (red data

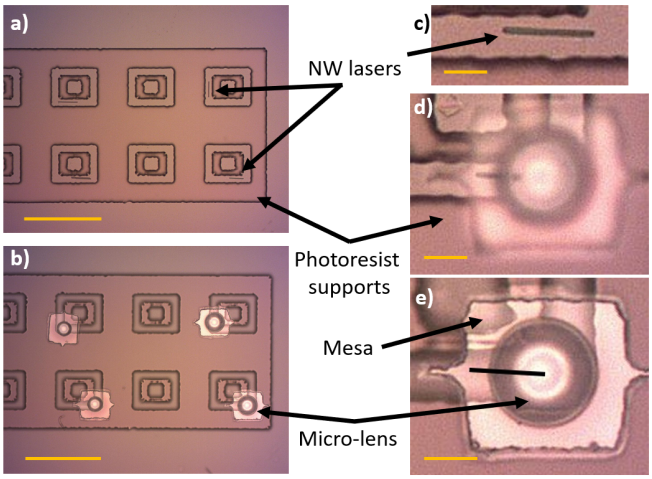

Fig. 8. Optical microscope images of the vertical assembly of InP NWs with GaN micro-lens membranes. (a) Large area view of NWs printed between polymer support frames and (b) after integration of the semiconductor micro-lenses. Scale bars are 50 μm. (c) Magnified view of a representative NW printed between the polymer frames (scale bar 5 μm). (d) and (e) show optical microscope images of the NW after integration of the micro-lens where the microscope focus plane coincides with the NW and top surface of the micro-lens respectively (scale bars 6 μm). The NW location, with one facet aligned to the centre of the lens, in (e) is added using image overlay as a guide to the eye.

points and line), for the NW laser shown in Fig. 8(c-e). Finally, the NWs are optically characterised again after integration of the lens structures. To maintain consistent pumping conditions, the pump laser spot is applied through the mesa region of the micro-lens membrane. Nevertheless, some variation of the pumping conditions due to optical path differences through the lens and mesa structures can be expected, compared with the free space coupled case. The lasing threshold and emission wavelengths of the fully assembled devices were consistent with measurements before addition of the lens, with a stable lasing threshold fluence measured at 20 $\mu J/cm^2$ and

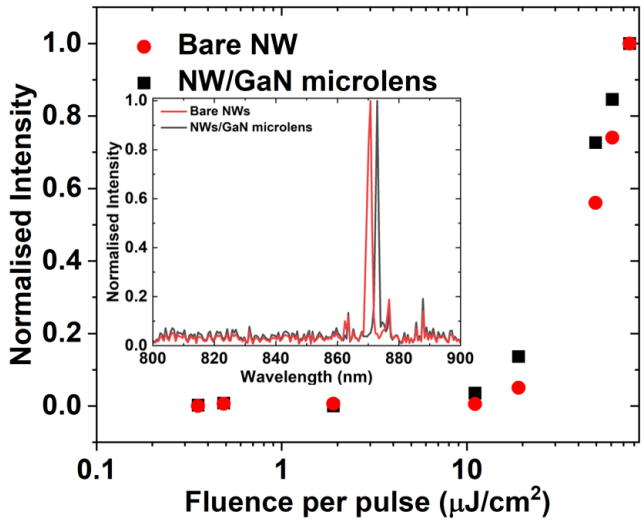

Fig. 9. Representative NW laser with and without micro-lens collection optics showing lasing threshold fluence and, inset, associated emission spectrum.

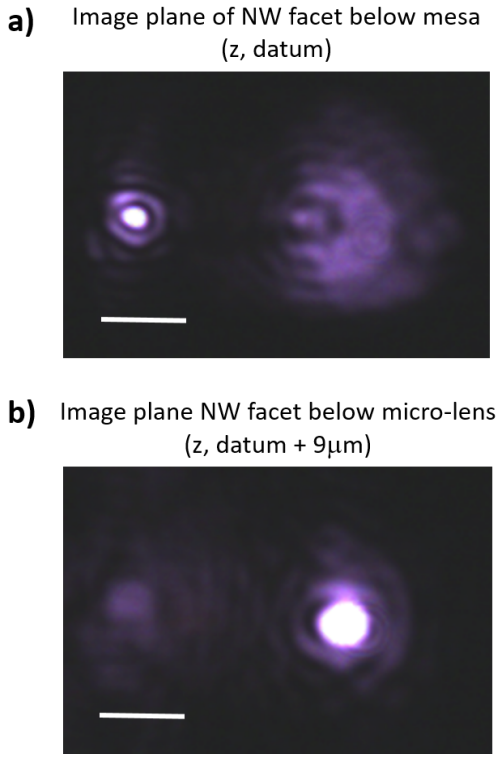

Fig. 10. (a) Microscope images of the NW laser with integrated micro-lens under lasing conditions, where the microscope image plane coincides with (a) the near field of the NW facet coupling through the mesa area and (b) the focal plane of the NW facet coupling through the micro-lens. Scale bars 5 μm.

a wavelength of 872.9 nm. The small variation in lasing wavelength mostly likely corresponds to a change in dominant cavity mode that is common in these types of NW lasers [38].

The effect of including the lens was measured by imaging the emitted facet light from both ends of the NW, i.e. through the lens and through the planar mesa area of the lens membrane respectively. An initial measurement of the emitted light from the NW facet on-axis with the lens prior to lens integration was also taken. Fig. 10 shows NW emission optical microscope images corresponding to the focal plane of each facet of the NW after printing of the micro-lens. When imaging the NW facet under the mesa area of the membrane, the spot size and brightness is consistent with that measured when the NWs are emitting into free-space (Fig. 10(a)). The facet under the micro-lens structure, as expected, is imaged at a different focal plane of the microscope system (Fig. 10(b)). Furthermore, there is a clear magnification of the facet emission area through the lens as compared with the NW facets emission into free-space or through the mesa area of the lens. The increase in imaged spot diameter is a factor of $\approx$1.9 larger in the case of the facet coupled through the micro-lens. Integrating the intensity of the emitted facet spots with and without the lens structure, we find a factor of $approx$1.5 improvement in collection efficiency due to the addition of the lens.

V. Printing onto optical fibre, photonic integrated circuits and in-situ process monitoring

As noted in the introduction, one of the advantages of transfer printing as an integration technique is the possibility to assemble devices onto substrates beyond simple planar chips. In this work we present transfer printing of micron scale devices onto the facet of an optical fibre and the edge facet of an end-coupled photonic chip. Furthermore, we demonstrate that in-situ optical monitoring and calibration of the print process can be achieved using our optical injection module.

For non-planar substrates, the first consideration is sample mounting on the transfer print tool motion stage. Since the instrument was designed with long working distance microscope systems and an adjustable position stamp holder, there can be significant working space between the stamp head and motion stage surface for mounting intermediate jigs. Furthermore, the parallel kinematic motion of the stage system allows for definition of an arbitrary reference point for calculation of motion paths and spatial referencing. Therefore, a point in space above the stage surface can be defined coinciding with the printing surface to allow for ease of stage attitude calculation and motion control. In this work both an optical fibre and an edge coupled photonic chip were used as receiver devices and individual mounting jigs were fabricated for each case. These can be specifically tailored for the application using standard 3D printing technologies. Fig. 11(a) shows a schematic of the fibre mount system in-situ in the transfer printing tool. A photograph of the fibre mounted in the printing system is shown in Fig. 11(b) where the exposed fibre facet is visible under the PDMS stamp head of the system; and, inset, an in-situ optical microscope image of the optical fibre facet with white light injected at the far end of the fibre.

A. Printing onto optical fibre and in-situ process monitoring

Printing devices onto an optical fibre facet, in addition to demonstrating non-planar receiver compatibility, also provides the opportunity for in-situ optical monitoring of the printing system. As detailed above, the custom transfer print instrument incorporates an optical injection system, as shown in Fig. 1(a), that enables fibre coupled lasers or light sources to be scanned across the transfer print microscope imaging system field of view. In this way, light can be directly coupled to objects mounted on the motion control stage. Furthermore, by using optical fibre as the transfer print receiver, the far end of the fibre can be used to couple to a light source, allowing imaging of the illuminated fibre core in the transfer print system microscope camera, as shown in Fig. 12 (and inset of Fig. 11(b)). Here we present use cases for both illumination sources.

In the case where the remote fibre end is injected with a white light source, the fibre core becomes illuminated in the print tool FOV, making positional registration of the core possible. A GaN micro-lens, of the same design detailed above in Section IV, was picked up using the print stamp head and brought into coarse alignment with the optical fibre facet. By monitoring the imaged light from the fibre core, the relative alignment of the micro-lens and fibre core can be carried out in real-time as shown in Fig. 12(a), where a range of micro-lens positions are captured in mis-aligned states with the fibre core. The final image shows the case where micro-lens and fibre are well aligned and the fibre core light is imaged through the micro-lens, producing a clear, symmetric output spot with a focal diameter smaller than the bare fibre core, Fig. 12(b).

Sometimes it may not be possible to illuminate the remote end of the fibre, or on-chip structure, but instead access to the in-coupled light using photodetector, or a reflected light from the substrate, may be used. Under this condition, the optical injection setup in the transfer print instrument can be used to illuminate the structure of interest and the coupled light can be monitored to assess the alignment of the printing in-situ. We use the optical injection setup to illuminate the fibre core through the printing system and monitor the coupled light with a photodetector at the remote fibre end. Aligning a micro-lens to the fibre core in this case is more difficult since the structure is essentially invisible to the microscope imaging system. To overcome this limitation, the optical injection spot is fixed in position and the translation stage is scanned while the power received at the remote fibre end is monitored as a function of the stage (fibre core) position. Fig. 13(a) shows the measured photodetector ouptut as a function of lateral translations of the motion control stage in x and y directions from the initial coarsely aligned $(0, 0)$ position. The central peak intensity corresponds to the maximum optical power coupled through the fibre to the detector, i.e. when the fibre core and optical injection spot are aligned in the transfer print instrument. This peak in optical power then identifies alignment of the optical injection spot and the fibre core structure with reference to the motion stage coordinates. Care is taken to compensate for z-direction offset in lateral position coordinates during the print stage using optical injection calibration. Fig. 13(b) illustrates this process with the last image showing the released micro-lens on the illuminated fibre core after the calibrated release. Fig. 13(b)) illustrates this process with the last image showing the released micro-lens on the illuminated fibre core after the calibrated release.

B. Printing onto planar chip facets

As noted above, a micro-lens can be printed directly onto a flat single mode fibre core to improve optical coupling to highly confined on-chip optical structures. Alternatively, the micro-lens can be printed onto the edge facet of the waveguide chip as shown in Fig. 14(a). This is a challenging print geometry due to the compact size of the waveguide core and the facet positioning of the micro-lens. To demonstrate this concept we used a GaN-on-sapphire waveguide chip, where the GaN ridge waveguide is 1 μm in width and has a height of 650 nm, plus a further 350 nm of AlN buffer. Full material and fabrication details can be found in [30]. For the printing process the GaN waveguide sample was mounted in a vertical sub-mount with one facet acting as the receiver substrate for the transfer printing process. A GaN micro-lens device similar to those presented above was printed from its native GaN-on-silicon substrate onto the waveguide

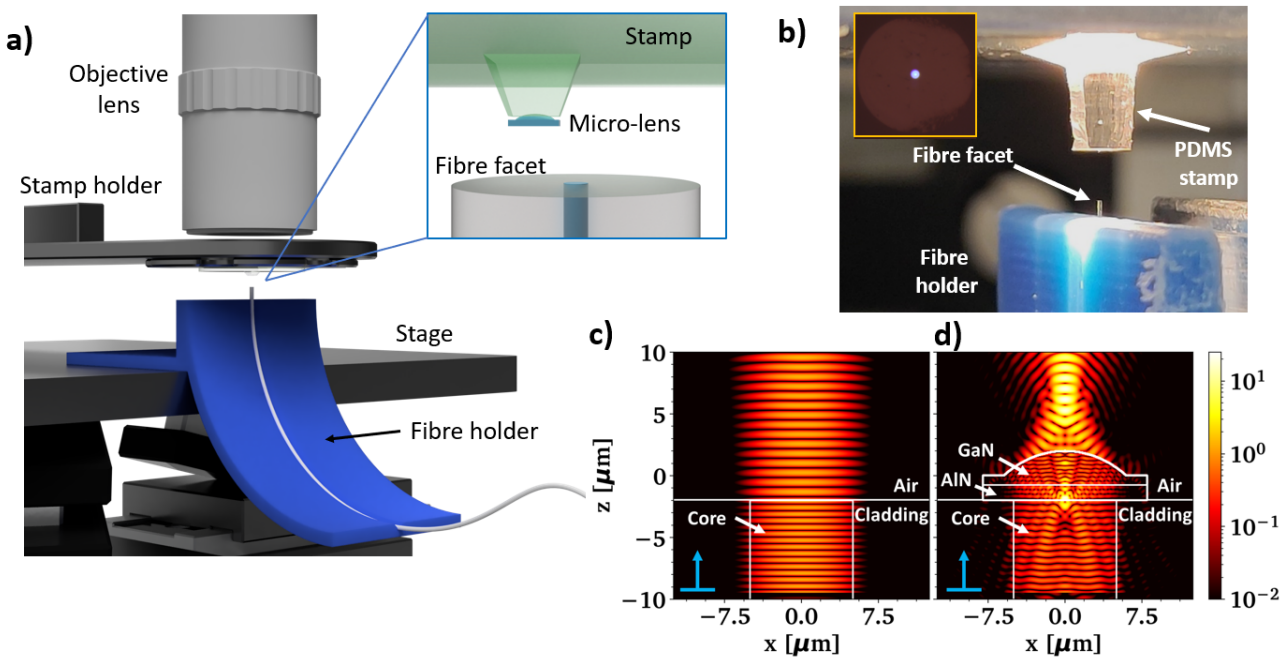

Fig. 11. Transfer printing onto the facet of an optical fibre: (a) schematic representation of the TP process and (b) in-situ photograph of the TP arrangement. (c) FDTD simulation of light coupling to free-space from a single mode fibre and (d) in the case of a micro-lens integrated onto the fibre facet.

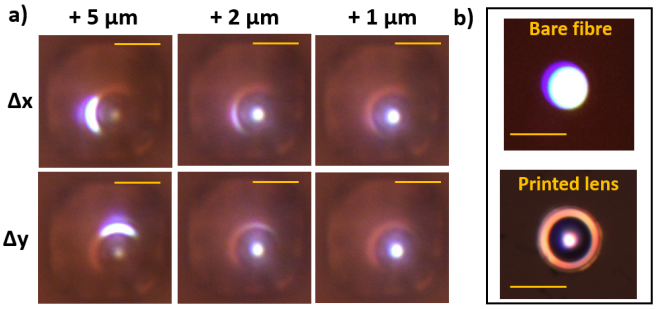

Fig. 12. Relative alignment of an optical fibre facet with a GaN micro-lens membrane with white light injected at the remote end of the fibre. (a) The micro-lens membrane on the stamp (stationary in FOV of the optical imaging system) is brought into few μm proximity of the illuminated fibre core, which is laterally shifted at various x and y positions. (b) micrograph showing in-situ measurement of the fibre facet emission before (top) and after (bottom) integration of the micro-lens membrane. Scale bars 15 μm.

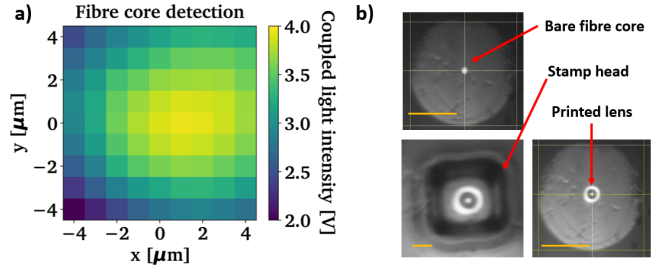

Fig. 13. (a) Photo-detector output intensity as a function of the fibre core position as scanned in the XY plane of the transfer print instrument. (b) In-situ optical microscope images of the fibre core (top), close-up of the micro-lens being printed (bottom left) and after the micro-lens is printed (bottom right). Scale bars 15 μm.

facet. Alignment between the waveguide and micro-lens was achieved using the waveguide cross-section and micro-lens circular aperture structure as spatial references in the fixed field of view microscopy imaging system. The central points of each structure were defined relative the motion control stage coordinates and the lens was translated while on the PDMS stamp to align its central axis with the centre of area of the waveguide cross section. Fig. 14(b) inset shows a microscope image of the edge facet of the GaN-on-sapphire waveguide chip prior to integration of the micro-lens. Fig. 14(b) shows the printed GaN lens on the same area of chip with the central lens aperture overlapping with the waveguide core. The micro-lens membrane diameter extends beyond the upper-cladding thickness of the waveguide chip, meaning that some of the material is suspended in air, showing that even small surface contact areas can allow for successful printing.

VI. Conclusion

An advanced transfer printing system incorporating real-time active optical monitoring and the ability to print onto non-standard substrates was presented. The use of parallel kinematic motion control stages enables flexible pose control of the stage and user defined motion paths around arbitrary spatial reference points. The optical imaging system operates with long working distances allowing for sub-mounts to be used on the motion control stage, and an optical injection line is implemented to allow coupling of optical sources with objects within the microscope field of view during the printing process. A number of demonstrator devices were presented, including micro-disk resonators printed onto micro-pillars and evanescently coupled to on-chip waveguides, inverted membrane device printing, and multi-layer print integration

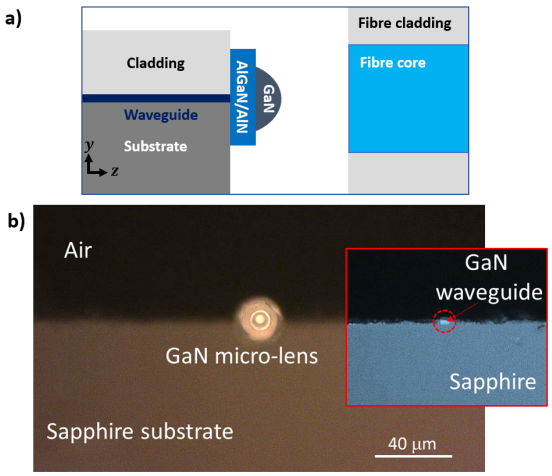

Fig. 14. (a) Schematic of fibre to planar waveguide coupling aided by a micro-lens printed onto the waveguide chip facet. (b) Optical microscope images of a GaN-on-sapphire planar waveguide facet with an integrated GaN/AlN micro-lens membrane device. (Inset: image of the waveguide facet before printing of the micro-lens).

incorporating NW lasers emitting through suspended semiconductor micro-lenses. Finally, in-situ optical monitoring of transfer printing of a micro-lens onto an optical fibre facet was demonstrated, both through back illumination from the fibre and forward illumination from the transfer print system. The flexibility of the stage mechanics and optical monitoring enable printing of micron scale devices onto non-standard substrates and allow for in-process measurements that will accelerate future systems integration and reduce potential rework.

ACKNOWLEDGMENT

The authors acknowledge Dr Q. Gao, Prof. L. Fu, Prof. H. Tan and Prof C. Jagadish at the ANU and the Australian National Fabricate Facility, ACT node for providing NW samples. The authors acknowledge support from the Royal Academy of Engineering (Research Chairs and Senior Research Fellowships); Engineering and Physical Sciences Research Council (EP/P013597/1, EP/R03480X/1, EP/V004859/1, EP/N017927/1, EP/P00945X/1);Innovate UK (50414); DSTL (DSTLX-1000146956) and the Fraunhofer Lighthouse Project QMag. S.P Bommer acknowledges PhD support from DSTL (DSTLX-1000140959) and Z. Xia and N.K. Wessling from Fraunhofer UK.

REFERENCES

[1] G.-H. Duan, C. Jany, A. L. Liepvre, A. Accard, M. Lamponi, D. Make, P. Kaspar, G. Levaufre, N. Girard, F. Lelarge, J.-M. Fedeli, A. Descos, B. B. Bakir, S. Messaoudene, D. Bordel, S. Menezo, G. de Valicourt, S. Keyvaninia, G. Roelkens, D. V. Thourhout, D. J. Thomson, F. Y. Gardes, and G. T. Reed, "Hybrid $III-V$ on silicon lasers for photonic integrated circuits on silicon," *IEEE J. Sel. Top. Quantum Electron.*, vol. 20, pp. 158–170, 2014.

[2] G. Muliuk, N. Ye, J. Zhang, A. Abbasi, A. Trindade, C. Bower, D. Van Thourhout, and G. Roelkens, "Transfer Print Integration of 40Gbps Germanium Photodiodes onto Silicon Photonic ICs," *European Conference on Optical Communication, ECOC*, vol. 2017-Sept, no. 3, pp. 1–3, 2017.

[3] J. Zhang, A. De Groote, A. Abbasi, R. Loi, J. O'Callaghan, B. Corbett, A. J. Trindade, C. A. Bower, and G. Roelkens, "Silicon photonics fiber-to-the-home transceiver array based on transfer-printing-based integration of $III-V$ photodetectors," *Optics Express*, vol. 25, no. 13, p. 14290, 2017.

[4] J.-H. Kim, S. Aghaeimeibodi, J. Carolan, D. Englund, and E. Wak, "Hybrid integration methods for on-chip quantum photonics," *Optica*, vol. 7, p. 291, 2020.

[5] A. W. Elshaari, A. Skalli, S. Gyger, M. Nurizzo, L. Schweickert, I. E. Zadeh, M. Svedendahl, S. Steinhauer, and V. Zwiller, "Deterministic integration of hBN emitter in silicon nitride photonic waveguide," *Adv. Quantum Technol.*, vol. 4, p. 2100032, 2021.

[6] J. H. Kim, S. Aghaeimeibodi, C. J. Richardson, R. P. Leavitt, D. Englund, and E. Waks, "Hybrid Integration of Solid-State Quantum Emitters on a Silicon Photonic Chip," *Nano Letters*, vol. 17, no. 12, pp. 7394–7400, 2017.

[7] S.-I. Park, Y. Xiong, R.-H. Kim, P. Elvikis, M. Meitl, D.-H. Kim, J. Wu, J. Yoon, C.-J. Yu, Z. Liu, Y. Huang, K. chih Hwang, P. Ferreira, X. Li, K. Choquette, and J. Rogers, "Printed assemblies of inorganic light-emitting diodes for deformable and semi-transparent displays," *Science*, vol. 325, pp. 977–981, 2009.

[8] C. Bower, M. Meitl, B. Raymond, E. Radauscher, R. Cok, S. Bonafede, D. Gomez, T. Moore, C. Prevatte, B. Fisher, R. Rotzoll, G. Melnik, A. Fecioru, and A. Trindade, "Emissive displays with transfer-printed assemblies of 8 $\mu m \times 15$ μm inorganic light-emitting diodes," *Photonics Research*, vol. 5, pp. A23–A29, 2017.

[9] J. O'Callaghan, R. Loi, E. E. Mura, B. Roycroft, A. J. Trindade, K. Thomas, A. Gocalinska, E. Pelucchi, J. Zhang, G. Roelkens, C. A. Bower, and B. Corbett, "Comparison of InGaAs and InAlAs sacrificial layers for release of InP-based devices," *Optical Materials Express*, vol. 7, no. 12, p. 4408, 2017.

[10] B. Corbett, R. Loi, W. Zhou, D. Liu, and Z. Ma, "Transfer print techniques for heterogeneous integration of photonic components," *Progress in Quantum Electronics*, vol. 52, pp. 1–17, 2017.

[11] D. Gomez, K. Ghosal, M. A. Meitl, S. Bonafede, C. Prevatte, T. Moore, B. Raymond, D. Kneeburg, A. Fecioru, A. J. Trindade, and C. A. Bower, "Process Capability and Elastomer Stamp Lifetime in Micro Transfer Printing," *Proceedings - Electronic Components and Technology Conference*, vol. 2016-August, pp. 680–687, 2016.

[12] J. Zhang, G. Muliuk, J. Juvert, S. Kumari, J. Goyvaerts, B. Haq, C. Op De Beeck, B. Kuyken, G. Morthier, D. Van Thourhout, R. Baets, G. Lepage, P. Verheyen, J. Van Campenhout, A. Gocalinska, J. O'Callaghan, E. Pelucchi, K. Thomas, B. Corbett, A. J. Trindade, and G. Roelkens, "$III-V-on-Si$ photonic integrated circuits realized using micro-transfer-printing," *APL Photonics*, vol. 4, no. 11, 2019.

[13] C. Op de Beeck, F. M. Mayor, S. Cuyvers, S. Poelman, J. F. Herrmann, O. Atalar, T. P. McKenna, B. Haq, W. Jiang, J. D. Witmer, G. Roelkens, A. H. Safavi-Naeini, R. Van Laer, and B. Kuyken, "$III-V-on-$lithium niobate amplifiers and lasers," *Optica*, vol. 8, no. 10, p. 1288, 2021.

[14] L. Liu, R. Loi, B. Roycroft, J. O'Callaghan, A. J. Trindade, S. Kelleher, A. Gocalinska, K. Thomas, E. Pelucchi, C. A. Bower, and B. Corbett, "Low-power-consumption optical interconnect on silicon by transfer-printing for used in opto-isolators," *Journal of Physics D: Applied Physics*, vol. 52, no. 6, 2019.

[15] A. Osada, Y. Ota, R. Katsumi, K. Watanabe, S. Iwamoto, and Y. Arakawa, "Transfer-printed quantum-dot nanolasers on a silicon photonic circuit," *Applied Physics Express*, vol. 11, p. 72002, 2018.

[16] J. Yoon, S.-M. Lee, D. Kang, M. Meitl, C. Bower, and J. Rogers, "Heterogeneously integrated optoelectronic devices enabled by micro-transfer printing," *Adv. Optical Mater.*, vol. 3, pp. 1313–1335, 2015.

[17] D. Jevtics, J. Smith, J. McPhillimy, B. Guilhabert, P. Hill, C. Klitis, A. Hurtado, M. Sorel, H. Tan, C. Jagadish, M. D. Dawson, and M. Srtain, "Spatially dense integration of micron-scale devices from multiple materials on a single chip via transfer printing," *Opt. Mater. Express*, vol. 11, pp. 3567–3576, 2021.

[18] S. Kim, J. Wu, A. Carlson, S. Jin, A. Kovalsky, P. Glass, Z. Liu, N. Ahmed, S. Elgan, W. Chen, P. Ferreira, M. Sitti, Y. Huang, and J. Rogers, "Microstructured elastomeric surfaces with reversible adhesion and examples of their use in deterministic assembly by transfer printing," *PNAS*, vol. 107, pp. 17 095–17 100, 2010.

[19] A. Carlson, A. bowen, Y. Huang, R. Nuzzo, and J. Rogers, "Transfer printing techniques for materials assembly and micro-nanodevice fabrication," *Adv. Mater.*, vol. 24, pp. 5284–5318, 2012.

[20] K. Aoki, H. T. Miyazaki, H. Hirayama, K. Inoshita, T. Baba, K. Sakoda, N. Shinya, and Y. Aoyagi, "Microassembly of semiconductor three-

dimensional photonic crystals," *Nature Materials*, vol. 2, pp. 117–121, 2003.
[21] C. Linghu, S. Zhang, C. Wang, and J. Song, "Transfer printing techniques for flexible and stretchable inorganic electronics," *npj Flexible Electronics 2018 2:1*, vol. 2, no. 1, pp. 1–14, 2018.
[22] "SYLGARD™ 184 Silicone Elastomer Kit." [Online]. Available: https://www.dow.com/en-us/pdp.sylgard-184-silicone-elastomer-kit.01064291z.html{\#}overview
[23] J. McPhillimy, D. Jevtics, B. Guilhabert, C. Klitis, A. Hurtado, M. Sorel, and M. D. Dawson, "Automated nanoscale absolute accuracy alignment system for transfer printing," *ACS Applied Nano Materials*, vol. 3, no. 10, pp. 10 326–10 332, 2020.
[24] S. B. Papp, K. Beha, P. DelHaye, F. Quinlan, H. Lee, K. J. Vahala, and S. A. Diddams, "A microresonator frequency comb optical clock," *Optica*, vol. 1, no. 1, pp. 10–14, 2013.
[25] J. Chiles, N. Nader, E. J. Stanton, D. Herman, G. Moody, J. Zhu, J. Connor Skehan, B. Guha, A. Kowligy, J. T. Gopinath, K. Srinivasan, S. A. Diddams, I. Coddington, N. R. Newbury, J. M. Shainline, S. W. Nam, and R. P. Mirin, "Multifunctional integrated photonics in the mid-infrared with suspended AlGaAs on silicon," p. 1246, 2019.
[26] A. Kovach, D. Chen, J. He, H. Choi, A. H. Dogan, M. Ghasemkhani, H. Taheri, and A. M. Armani, "Emerging material systems for integrated optical Kerr frequency combs," *Advances in Optics and Photonics*, vol. 12, no. 1, p. 135, 2020.
[27] S. W. Park, M. W. Kim, K. T. Park, J. H. Ku, and Y. S. No, "On-Chip Transferrable Microdisk Lasers," *ACS Photonics*, vol. 7, pp. 3313–3320, 2020.
[28] B. Guilhabert, J. McPhillimy, S. May, C. Klitis, M. D. Dawson, M. Sorel, and M. J. Strain, "Hybrid integration of an evanescently coupled AlGaAs microdisk resonator with a silicon waveguide by nanoscale-accuracy transfer printing," *Optics Letters*, vol. 43, no. 20, p. 4883, 2018.
[29] J. McPhillimy, B. Guilhabert, C. Klitis, M. D. Dawson, M. Sorel, and M. J. Strain, "High accuracy transfer printing of single-mode membrane silicon photonic devices," *Opt. express*, vol. 26, p. 16679, 2018.
[30] J. Smith, P. Hill, C. Klitis, L.Weituschat, P. Postigo, M. Sorel, M. Dawson, and M. Strain, "High precision integrated photonic thermometry enabled by a transfer printed diamond resonator on gan waveguide chip," *Opt. express*, vol. 29, pp. 29 095–29 106, 2021.
[31] D. Jevtics, B. Guilhabert, A. Hurtado, M. D. Dawson, and M. J. Strain, "Deterministic integration of single nanowire devices with on-chip photonics and electronics," *Progress in Quantum Electronics*, p. 100394, 2022.
[32] A. Trindade, B. Guilhabert, D. Massoubre, D. Zhu, N. Laurand, E. Gu, I. Watson, C. Humphreys, and M. Dawson, "Nanoscale-accuracy transfer printing of ultra-thin $AlInGaN$ light-emitting diodes onto mechanically flexible substrates," *Appl. Phys. Lett.*, vol. 103, p. 253302, 2013.
[33] T. Tajiri, S. Takahashi, Y. Ota, K. Watanabe, S. Iwamoto, and Y. Arakawa, "Three-dimensional photonic crystal simultaneously integrating a nanocavity laser and waveguides," *Optica*, vol. 6, p. 296, 2019.
[34] N. H. Wan, T. J. Lu, K. C. Chen, M. P. Walsh, M. E. Trusheim, L. De Santis, E. A. Bersin, I. B. Harris, S. L. Mouradian, I. R. Christen, E. S. Bielejec, and D. Englund, "Large-scale integration of artificial atoms in hybrid photonic circuits," *Nature*, vol. 583, no. 7815, pp. 226–231, 2020.
[35] D. Jevtics, J. McPhillimy, B. Guilhabert, J. Alanis, H. Tan, , C. Jagadish, M. D. Dawson, A. Hurtado, P. Parkinson, and M. Srtain, "Characterization, selection, and microassembly of nanowire laser systems," *Nano. Lett.*, vol. 20, pp. 1862–1868, 2020.
[36] B. Spiridon, M. Toon, A. Hinz, S. Ghosh, S. Fairclough, B. Guilhabert, M. Strain, I. Watson, M. Dawson, D. Wallis, and R. Oliver, "Method for inferring the mechanical strain of $GaN-on-Si$ epitaxial layers using optical profilometry and finite element analysis," *Opt. Mater. Express*, vol. 11, pp. 1643–1655, 2021.
[37] N. Wessling, S. Ghosh, B. Guilhabert, M. Kappers, R. Oliver, M. Dawson, and M. Strain, "Fabrication and transfer print based integration of free-standing GaN membrane micro-lenses onto semiconductor chips," *arXiv*, vol. arXiv:2208.05275v1, 2022.
[38] S. A. Church, R. Al-Abri, P. Parkinson, and D. Saxena, "Optical characterisation of nanowire lasers," *Progress in Quantum Electronics*, p. 100408, 2022.

Benoit Guilhabert Benoit Guilhabert received his Engineering diploma from the Ecole Nationale d'Ingénieurs du Mans, France, a MSc in integrated photonics sensors from the Université du Maine, France and his PhD from the University of Strathclyde, UK. He is currently a Research Fellow at the University of Strathclyde where he focuses on heterogeneous integration.

Sean Bommer Sean Bommer received the MPhys Degree in Physics with specialisation in Photonics from the University of Strathclyde. He is currently working towards his doctorate on hybrid integration of nominally identical resonators for photon-pair generation with the integrated photonics group in the University of Strathclyde.

Nils K. Wessling Nils K. Wessling received a MSc degree in Physics from the University of Münster, Germany, gaining expertise in optical spectroscopy of 2D materials and in system development for the European XFEL and FLASH at Desy in Hamburg, Germany. He is currently pursuing his PhD in Michael Strain's group at the University of Strathclyde in Glasgow, UK. His work focuses on the fabrication, modelling and integration of GaN micro-lenses.

Dimitars Jevtics Dimitars Jevtics received his MEng in electronic engineering and nanotechnology from the University of York (UK) in 2015. He joined the Institute of Photonics at the University of Strathclyde (UK) to pursue his PhD where he is currently working as a research associate in the Integrated Optics group. His research is focused on the deterministic integration of semiconductor nanowire lasers with nano-photonic components using the techniques of micro-transfer-printing.

Jack A. Smith Jack A Smith received a BSc(Hons) in Physics from the University of Aberdeen in 2015, and an MSc in Diamond Science and Technology from the University of Warwick in 2017. He is presently a PhD candidate at the University of Strathclyde. His research interests include photonic integrated circuits fabricated in wide-bandgap materials and heterogeneous integration.

Zhongyi Xia Zhongyi Xia received a BEng in Electronic Engineering and an MSc degree in Semiconductor Photonics and Electronics both from the University of Sheffield. He is now pursuing the PhD degree in the University of Strathclyde, Glasgow. His research is focused on fabrication of high-speed, high-density micro-LED based SLMs via transfer-printing technology.

Saptarsi Ghosh Saptarsi Ghosh (Member IEEE) received the MTech degree from Jadavpur University, India, and the PhD degree from IIT Kharagpur, India. He is presently a Research Associate at the Cambridge Centre for Gallium Nitride. His current research interests include MOCVD growth of III-nitrides and physics of low-dimensional microelectronics devices.

Menno Kappers *Biography unavailable at the time of submission.*

Ian M. Watson Ian M. Watson received the BA (Hons) degree from the University of Cambridge, UK, in 1984, and the PhD degree in materials chemistry from the University of Kent, UK, in 1989. He has researched III-nitride materials and devices at Strathclyde University since 1998, leading an III-nitride MOVPE crystal growth activity in the period 2000-2008. He has experience outside academia at Plessey Research (1984-1986) and at EEV Ltd. (1995-1998), in addition to pursuing postdoctoral research on MOVPE at the University of Cambridge then the University of London (1989-1995).

Rachel A. Oliver Prof. Rachel Oliver FREng received her MEng (2000) and PhD (2003) degrees from the University of Oxford, UK. She then moved to Cambridge as a Research Fellow at Peterhouse College, and later won a Royal Society University Research Fellowship. In 2011, she took up her permanent academic position at the University of Cambridge and she is currently Professor of Materials Science and Director of the Cambridge Centre for Gallium Nitride. She held a Leverhulme Senior Research Fellowship in 2015-2016 and delivered the Rank Prize Lecture in Photonics in 2018. She was one of the Women in Engineering Society's Top 50 Women in Engineering in 2020 and was elected Fellow of the Royal Academy of Engineering in 2021.

Martin D. Dawson Prof. Martin D. Dawson (Fellow, IEEE) is a Physicist known for his work on lasers and compound semiconductors. He is the Director of Research with the Institute of Photonics, University of Strathclyde, Glasgow, U.K., which he helped to establish 26 years ago, and he was also appointed as the Inaugural Head of the Fraunhofer Centre for Applied Photonics in October 2012. He has more than 35 years' experience of applied research gained in academia and industry in the U.K. and the USA, and he has been involved in the formation and technical development of a number of spin-out businesses, most recently including mLED Ltd. He was the recipient of the 2016 Aron Kressel Award and the 2021 Distinguished Service Award from the IEEE Photonics Society, and the 2021 Nick Holonyak Jr. Award from Optica.

Michael J. Strain Prof. Michael J. Strain (Senior Member IEEE) received an MEng in Electrical and Mechanical Engineering, MASc and PhD degrees in Photonics from the Universities of Strathclyde, Toronto and Glasgow respectively. He currently holds the Fraunhofer UK / RAEng Research Chair in Chipscale Photonics at the University of Strathclyde. His group focuses on technologies for heterogeneous integration of integrated photonics with work covering non-linear optics, wide-bandgap semiconductors, sensors and opto-electronic integration.